

Metal substrates-induced phase transformation of monolayer transition metal dichalcogenides for hydrogen evolution catalysis

Zhe Wang(王喆) and Wenguang Zhu(朱文光)
Citation: Chin. Phys. B, 2021, 30 (**11**): 116401. DOI: 10.1088/1674-1056/abfbd1
Journal homepage: http://cpb.iphy.ac.cn; http://iopscience.iop.org/cpb

What follows is a list of articles you may be interested in

Novel structures and mechanical properties of Zr_2N: *Ab initio* description under high pressures

Minru Wen(文敏儒), Xing Xie(谢兴), Zhixun Xie(谢植勋), Huafeng Dong(董华锋), Xin Zhang(张欣), Fugen Wu(吴福根), and Chong-Yu Wang(王崇愚)
Chin. Phys. B, 2021, 30 (**1**): 016403. DOI: 10.1088/1674-1056/abb220

Thickness-dependent structural stability and transition in molybdenum disulfide under hydrostatic pressure

Jiansheng Dong(董健生), Gang Ouyang(欧阳钢)
Chin. Phys. B, 2020, 29 (**8**): 086403. DOI: 10.1088/1674-1056/ab9440

Anomalous behavior and phase transformation of α -GaOOH nanocrystals under static compression

Zhao Zhang(张钊), Hang Cui(崔航), Da-Peng Yang(杨大鹏), Jian Zhang(张剑), Shun-Xi Tang(汤顺熙), Si Wu(吴思), Qi-Liang Cui(崔啟良)
Chin. Phys. B, 2017, 26 (**10**): 106402. DOI: 10.1088/1674-1056/26/10/106402

Low-temperature phase transformation of CZTS thin films

Wei Zhao(赵蔚), Lin-Yuan Du(杜霖元), Lin-Lin Liu(刘林林), Ya-Li Sun(孙亚利), Zhi-Wei Liu(柳志伟), Xiao-Yun Teng(滕晓云), Juan Xie(谢娟), Kuang Liu(刘匡), Wei Yu(于威), Guang-Sheng Fu(傅广生), Chao Gao(高超)
Chin. Phys. B, 2017, 26 (**4**): 046402. DOI: 10.1088/1674-1056/26/4/046402

Structure phase transformation and equation of state of cerium metal under pressures up to 51 GPa

Ce Ma(马策), Zuo-Yong Dou(窦作勇), Hong-Yang Zhu(祝洪洋), Guang-Yan Fu(付广艳), Xiao Tan(谈笑), Bin Bai(白彬), Peng-Cheng Zhang(张鹏程), Qi-Liang Cui(崔啟良)
Chin. Phys. B, 2016, 25 (**4**): 046401. DOI: 10.1088/1674-1056/25/4/046401

Metal substrates-induced phase transformation of monolayer transition metal dichalcogenides for hydrogen evolution catalysis*

Zhe Wang(王喆)[1,2,3] and Wenguang Zhu(朱文光)[1,2,3,†]

[1] Department of Physics, University of Science and Technology of China, Hefei 230026, China
[2] International Center for Quantum Design of Functional Materials (ICQD), Hefei National Laboratory for Physical Sciences at the Microscale, and Synergetic Innovation Center of Quantum Information and Quantum Physics, University of Science and Technology of China, Hefei 230026, China
[3] Key Laboratory of Strongly-Coupled Quantum Matter Physics, Chinese Academy of Sciences, School of Physical Sciences, University of Science and Technology of China, Hefei 230026, China

(Received 13 February 2021; revised manuscript received 12 April 2021; accepted manuscript online 27 April 2021)

Monolayer transition metal dichalcogenides can normally exist in several structural polymorphs with distinct electrical, optical, and catalytic properties. Effective control of the relative stability and transformation of different phases in these materials is thus of critical importance for applications. Using density functional theory calculations, we investigate the effects of low-work-function metal substrates including Ti, Zr, and Hf on the structural, electronic, and catalytic properties of monolayer MoS_2 and WS_2. The results indicate that such substrates not only convert the energetically stable structure from the 1H phase to the 1T′/1T phase, but also significantly reduce the kinetic barriers of the phase transformation. Furthermore, our calculations also indicate that the 1T′ phase of MoS_2 with Zr or Hf substrate is a potential catalyst for the hydrogen evolution reaction.

Keywords: transition metal dichalcogenides, phase transformation, hydrogen evolution reaction, density functional theory

PACS: 64.70.Nd, 71.20.–b, 81.16.Hc **DOI:** 10.1088/1674-1056/abfbd1

1. Introduction

Transition metal dichalcogenides (TMDs), as a class of representative layered materials, received tremendous research attention in recent years owing to their rich electronic, optical, and catalytic properties.[1–5] In the atomic structures of TMDs, each monolayer contains a transition-metal layer sandwiched between two chalcogenide layers. The variation in the stacking geometry of the three atomic layers may leads to different phases, typically a trigonal prismatic phase (1H) and an octahedral phase (1T). An intriguing feature of monolayer TMDs is their electronic structures critically depending on the atomic-layer stacking geometry. For group-VI-element TMDs MoS_2, its trigonal prismatic phase is a good semiconductor with a sizable bandgap, whereas its octahedral phase becomes metallic. This transition can be qualitatively understood as the difference in the splitting and filling of the transition-metal d-orbital dominated energy bands due to the different crystal symmetries and coordination environments of the two phases.[6] Such distinct electronic structures may in turn lead to disparate physical and chemical properties, such as catalytic activity. Although both 1H- and 1T-MoS_2 has shown to be catalytic for the hydrogen evolution reaction (HER), the active sites are solely limited at the edges in the 1H phase[7,8] but include the whole basal plane of the 1T phase.[9–14] However, for pristine MoS_2, the 1T phase is energetically less stable than the 1H phase. Therefore, to enhance the catalytic performance of MoS_2, it is highly desirable to increase the ratio of the 1T phase via tuning the relative stability of the two phases.

In this effort, there have been extensive attempts to induce structural phase transformation of group-VI elements Mo- and W-based TMDs and stabilize the 1T phase.[15–18] The main strategy of these research is to dope extra electrons into the TMDs via, for example, Re doping[19] and alkali ion intercalation.[20–23] Some other approaches including mechanical stress[24] and metal substrates[25–27] have also been reported. However, the stability of the obtained 1T phase still needs to be improved.[28,29] In addition, for the catalytic purpose, it is also vitally important to leave the active sites open for chemical reaction.

In this work, we use first-principles density functional theory (DFT) calculations to investigate the effects of three low-work-function metal substrates including Ti, Zr, and Hf on the structural, electronic, and catalytic properties of monolayer MoS_2 and WS_2. A distorted 1T phase, named 1T′ phase, is identified to become energetically most stable in the presence of the metal substrates. The electronic structure analysis indicates that the metal substrates donate electrons to the MoS_2 and WS_2 monolayers, leading to the phase transforma-

*Project supported by the National Key Research and Development Program of China (Grant Nos. 2017YFA0204904 and 2019YFA0210004), the Strategic Priority Research Program of the Chinese Academy of Sciences (Grant No. XDB30000000), and the Fundamental Research Funds for the Central Universities, China (Grant No. WK3510000013).

†Corresponding author. E-mail: wgzhu@ustc.edu.cn

© 2021 Chinese Physical Society and IOP Publishing Ltd

tion. Meanwhile, the presence of the substrates also significantly reduces the kinetic barriers of the phase transformation. In addition, Gibbs free energy calculations suggest that the HER catalytic activity on the top surface of the 1T′-MoS_2 monolayers is still largely preserved as placed on the Zr or Hf substrate.

2. Computational methods

The first-principles DFT calculations were performed using the Vienna *ab initio* simulation package (VASP).[30] Core and valence electrons were described using the projector-augmented wave (PAW) method.[31,32] The exchange and correlation functional was treated using the Perdew–Burke–Ernzerhof (PBE) parametrization of generalized gradient approximation (GGA) for structural relaxations and total energy calculations.[33] The energy cut-off of the plane wave basis was set to 300 eV. Electronic minimization was performed with a tolerance of 10^{-4} eV, and ionic relaxation was performed with a force tolerance of 0.01 eV/Å on each ion. A vacuum region more than 15 Å was used to ensure decoupling between neighboring slabs. A Γ-centered $18\times18\times1$ Monkhorst–Pack[34] k-mesh was used for k-point sampling. The climbing image nudged elastic band (CI-NEB) method[35] was used to determine the minimum energy pathways of the various kinetic processes and their transition states with five intermediate geometries (images) interpolated between the initial and the final states, and the transition states were finally achieved by the optimized central image. In addition, the van der Waals corrections was included as parameterized in the semiempirical DFT-D3(BJ) method.[36,37]

The binding energies of H adsorbed were calculated as $\Delta E_{\rm H} = E\,({\rm TMDs+H}) - E\,({\rm TMDs}) - \frac{1}{2}E({\rm H_2})$, where $E\,({\rm TMDs+H})$, $E\,({\rm TMDs})$, and $E({\rm H_2})$ are the total energies for the H adsorbed monolayer MoS_2 (WS_2) with or without the substrates, monolayer MoS_2 (WS_2) with or without the substrates, and H_2 in the gas phase, respectively. The Gibbs free energy was calculated by adding a thermal correction to the binding energy, which is defined by $\Delta G_{\rm H} = \Delta E_{\rm H} + \Delta E_{\rm ZPE} - T\Delta S_{\rm H}$, where $\Delta E_{\rm ZPE}$ and $T\Delta S_{\rm H}$ are the differences in the zero-point energy and entropy contribution between the H adsorbed state and H_2 in the gas phase, respectively. It is assumed that the vibrational entropy in the adsorbed state is small enough to be negligible.[38] The last term is usually approximated as $T\Delta S_{\rm H} = -\frac{1}{2}TS({\rm H_2})$, where $S({\rm H_2})$ is the entropy of H_2 in the gas phase at standard conditions ($T = 298.15$ K, pressure $= 1$ atm, 1 atm $= 1.01325\times10^5$ Pa). The zero-point energy of hydrogen atoms in different phases of TMDs, adsorption of hydrogen atoms at different concentrations, and presence or absence of the metal substrates were tested. The results under different conditions changes very little and will not affect the main conclusions. The zero-point energy of hydrogen atoms adsorbed on the surface of the 1T′ phase was used for all the cases, and the Gibbs free energies were calculated as $\Delta G_{\rm H} = \Delta E_{\rm H} + 0.29$ eV, which is consistent with previous work.[12]

3. Results and discussion

3.1. Structures and structural stability of TMDs with substrates

Monolayer 1H- and 1T-MoS_2 (WS_2), as shown in Fig. 1, are both composed of three layers of atoms, and each atomic layer contains only one element stacking in a sequence of S–Mo(W)–S. All the atoms in each atomic layer are arranged into a close-packed triangular lattice. The difference between the two phases is their vertical stacking geometries. As shown in Figs. 1(b) and 1(d), respectively, the 1H phase follows an ABA stacking sequence, while the 1T phase forms an ABC stacking sequence. For freestanding MoS_2 and WS_2 monolayers, the 1H phase is energetically most stable with total energy differences of approximately 0.8 eV from the DFT calculations. In addition, the freestanding 1T-MoS_2 and 1T-WS_2 monolayers are metastable. A more stable phase, named 1T′ phase, can be derived from the high-symmetry 1T phase via local structural distortion, ending up with a 2×1 superstructure and a small band gap opening (Figs. 1(e) and 1(f)). The calculated total energy of the 1T′ phase is 0.25 eV/MoS_2 (0.32 eV/WS_2) lower than that of the 1T phase, whereas it is still higher than that of 1H phase by around 0.6 eV for monolayer MoS_2 (WS_2).

Three *hcp* metals, Ti, Zr, and Hf, are chosen to investigate the effects of low-work-function metal substrates on the structural stability and catalytic activity of monolayer MoS_2 and WS_2. The lattices of the (0001) surface of these metals (Figs. 1(g) and 1(h)) can nicely match with the in-plane lattices of MoS_2 and WS_2. The calculated lattice constants of MoS_2 and WS_2 in different phases and the metals along with their lattice mismatches are summarized in Table 1. The lattice mismatches between MoS_2 (WS_2) and Ti, Zr, and Hf are $\sim7.8\%$, $\sim1.5\%$, and $\sim0.4\%$, respectively. In the calculations of the combined systems, the lattices of MoS_2 and WS_2 are adjusted to match the optimal lattices of the metal substrates, unless otherwise specified.

Table 1. Calculated lattice constants of MoS_2 and WS_2 in different phases and the metal substrates along with their lattice mismatches.

	TMDs	Ti (2.94 Å)	Zr (3.24 Å)	Hf (3.20 Å)
MoS_2	1T (3.19Å)	−7.8%	+1.6%	+0.3%
	1H (3.18 Å)	−7.5%	+1.9%	+0.6%
WS_2	1T (3.21 Å)	−8.4%	+0.9%	−0.3%
	1H (3.19 Å)	−7.8%	+1.6%	+0.3%

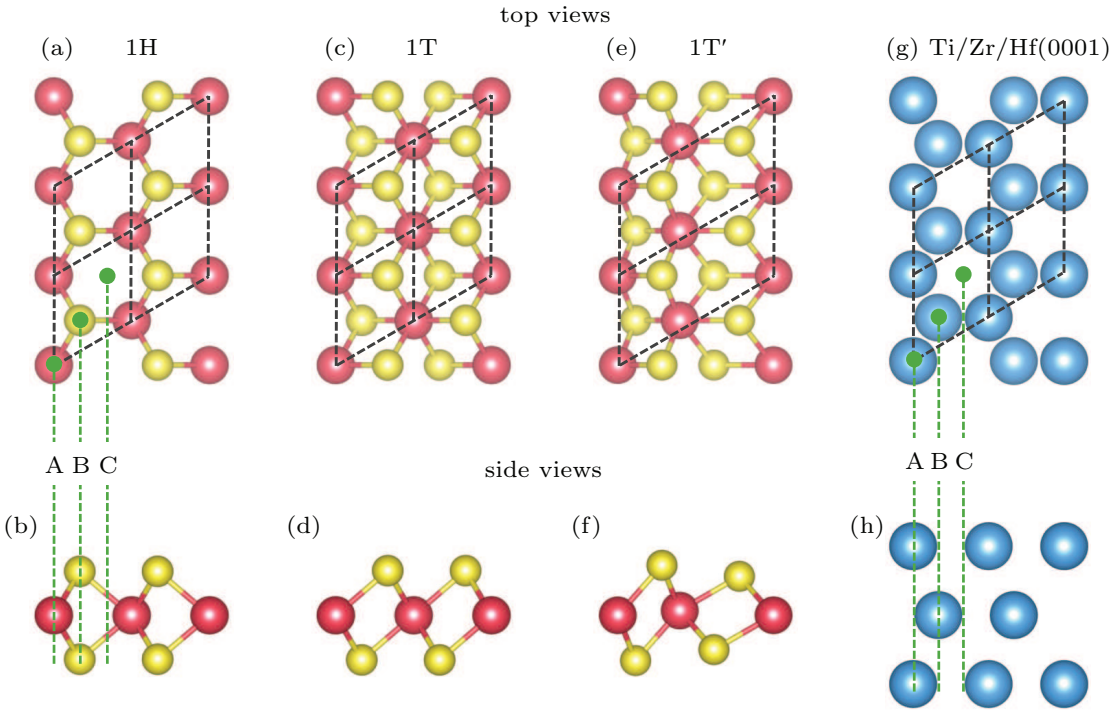
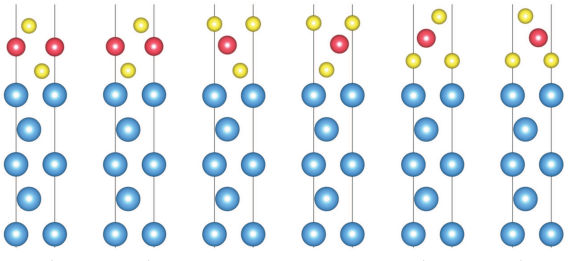


Fig. 1. Atomic structures of monolayer MoS_2 (WS_2), with Mo (W) atoms in red and S atoms in yellow, and the metal substrates, with the metal atoms in blue. (a)–(b) 1H phase. (c)–(d) 1T phase. (e)–(f) 1T′ phase. (g)–(h) Ti, Zr or Hf substrate. The sites of the metal atoms on the surface and second layer, and the hollow site are defined as A, B, and C, respectively.

To determine the most favorable stacking structures of the monolayer MoS_2 and WS_2 on the metal substrates, various possible high-symmetry stacking configurations are considered. For the (0001) surface terminated slabs of hcp metals, the atoms in each layer also form a triangular lattice, and the vertical stacking follows an ABAB sequence. To label different stacking configurations of the TMDs monolayers on the metal substrates, we denote the surface layer of the metal substrates as site A and the second layer as site B. The stacking configurations of the TMDs monolayers, as shown in Fig. 2, can be labeled as XY (X,Y = A, B, C), where X and Y correspond to the positions of the bottom S layer and the Mo atom with respect to the underlying metal substrate, respectively. The calculation results of the MoS_2/Hf system are summarized in the table of Fig. 2, which shows that for the 1H phase, the most favorable stacking configuration is BA, while it is CA for the 1T and 1T′ phases. More importantly, in contrast to the freestanding monolayer, the most stable structure of MoS_2 becomes the 1T′ phase in the presence of the Hf substrate.

To further examine the validity of our calculations, we thoroughly investigated the relative stability of various structural phases of MoS_2 and WS_2 on Ti, Zr, and Hf substrates with different settings of the lattice parameters using the optimal lattice constant of the metal substrate or the 1H- or 1T-TMDs monolayers. The calculated relative energies of different phases of MoS_2 and WS_2 in the two most likely configurations CA and BA on the metal substrates are summarized in Table 2. The results clearly confirm the above conclusion. The 1T′/1T phase of MoS_2 and WS_2 monolayers are always energetically more favorable than the 1H phase on these metal substrates. In the cases of using Ti as the substrate, the 1T′ phase becomes unstable exclusively as the lattice parameter is set to the lattice constant of Ti, because of a large compressive strain imposed on the TMDs monolayers. Instead, the structures were stabilized into the 1T phase, which still have lower energies than the 1H phase. Therefore, the proposed metal substrates can effectively reverse the relative thermaldynamic stability of monolayer MoS_2 and WS_2 from the 1H phase for the freestanding case to the 1T′/1T phase.



	CA	BA	CB	BC	AB	AC
1H (eV)	0.207	0.176	0.763	0.812	0.840	0.890
1T (eV)	0.096	0.162	0.751	0.890	1.315	1.389
1T′ (eV)	0	0.069	0.530	0.647	N/A	N/A

Fig. 2. Atomic structures of various possible high-symmetry stacking configurations and their relative energies in the MoS_2/Hf system. The different stacking configurations are labeled as XY (X,Y = A, B, C), where X and Y correspond to the positions of the bottom S layer and the Mo atom with respect to the underlying metal substrate, respectively. All data are the energies per MoS_2.

Table 2. Relative energies of various structural phases of MoS_2 and WS_2 with and without the metal substrates. The combined systems with different settings of the lattice parameters using the optimal lattice constant of the metal substrate or the 1H- or 1T-TMDs. The energies of each row are relative to the energy of the most stable structure in this row. All data are the energy per MoS_2 or WS_2.

MoS_2	Lattice	1H phase (eV)		1T phase (eV)		1T′ phase (eV)	
Freestanding	optimal	0		0.840		0.593	
Substrate		CA	BA	CA	BA	CA	BA
	Ti	0.156	0.132	0	0.066	N/A	N/A
Ti (0001)	1H	0.072	0.183	0.050	0.187	0	0.142
	1T	0.070	0.188	0.053	0.195	0	0.146
	Zr	0.190	0.149	0.105	0.158	0	0.038
Zr (0001)	1H	0.176	0.109	0.083	0.125	0	0.024
	1T	0.178	0.115	0.087	0.130	0	0.026
	Hf	0.207	0.176	0.096	0.162	0	0.069
Hf (0001)	1H	0.202	0.156	0.086	0.144	0	0.059
	1T	0.204	0.165	0.091	0.152	0	0.063
WS_2	Lattice	1H phase (eV)		1T phase (eV)		1T′ phase (eV)	
Freestanding	optimal	0		0.884		0.567	
Substrate		CA	BA	CA	BA	CA	BA
	Ti	0.108	0.067	0	0.066	N/A	N/A
Ti (0001)	1H	0.047	0.141	0.099	0.231	0	0.138
	1T	0.051	0.167	0.116	0.262	0	0.150
	Zr	0.192	0.124	0.170	0.212	0	0.022
Zr (0001)	1H	0.166	0.077	0.137	0.169	0	0.008
	1T	0.179	0.102	0.155	0.193	0	0.015
	Hf	0.203	0.140	0.149	0.202	0	0.053
Hf (0001)	1H	0.195	0.121	0.136	0.184	0	0.046
	1T	0.208	0.153	0.157	0.215	0	0.059

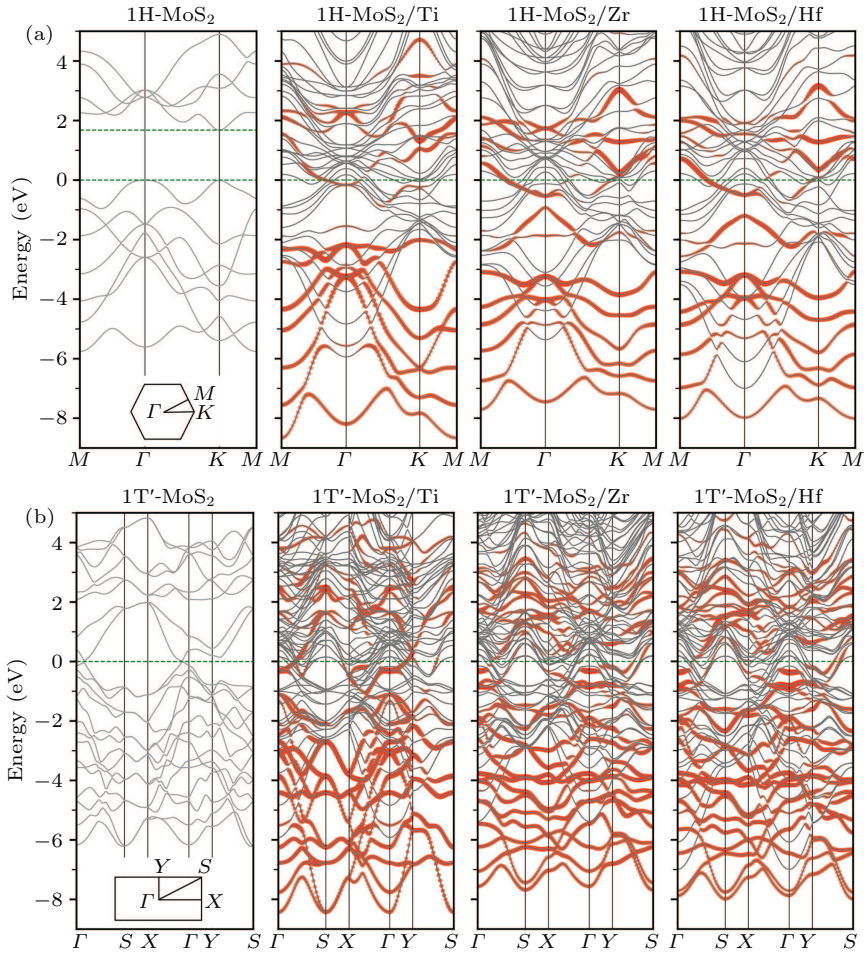


Fig. 3. Band structures of (a) 1H-MoS_2 and (b) 1T′-MoS_2 with and without the metal substrates, where the MoS_2 derived energy bands in the combined systems are highlighted in red.

The underlying mechanism of the metal substrate-induced phase stability reversal can be revealed from electronic structure analysis. Figure 3 shows the calculated band structures of 1H- and 1T′-MoS_2 monolayers on the three metal substrates, respectively, where the MoS_2 derived energy bands are highlighted in red. For comparison, the calculated band structures of freestanding MoS_2 monolayers in the 1H and 1T′ phases are also illustrated in Fig. 3. Although the energy bands of MoS_2 are modified to a certain extent in the combined systems due to the hybridization with the metal substrates, the positions of the original band edges of freestanding MoS_2 can still be identified. From these plots, it can be seen that for both 1H and 1T′ phases, the Fermi levels of the combined systems were always moved up into the original conduction bands of MoS_2, indicating the existence of effective electron transfer from the metal substrates to the MoS_2 monolayers. This observation is also consistent with our initial design of taking advantage of a low-work-function metal substrate to donate electrons into TMDs so as to reverse the relative stability from the 1H phase to the 1T′/1T phase.

3.2. Kinetics of phase transformation

Kinetics is also a key factor for the feasibility of phase transformation. In this regard, we investigated the kinetic processes and calculated the energy barriers of MoS_2 and WS_2 monolayers transforming from the 1H phase to the 1T phase in the presence of the metal substrates. Since the rate-limiting processes for the 1H phase to the 1T and 1T′ phases are essentially the same,[39] we use the 1T phase as the final state to simplify the calculation. The difference between 1H and 1T phases is the vertical alignment of the two chalcogen layers. The phase transformation thus can be achieved by simply moving one of the chalcogen layers collectively with respect to the other two atomic layers. However, when the TMDs monolayers placed on the metal substrates, the top and the bottom chalcogen layers become inequivalent, and thus there are two possible phase transformation pathways from the 1H phase to the 1T phase. For the 1H phase, the positions of the top and bottom S layer are both at the site B (defined in Fig. 1) with respect to the underlying metal substrate. The phase transformation from the 1H phase to the 1T phase can be achieved by simply moving the top or the bottom S layer from the site B to the site C. Figures 4(a) and 4(c) show the calculated energy profiles of the kinetic processes involving the moving of the top S layer. Compared with the cases of freestanding monolayers, the energy barriers are effectively reduced from ∼ 1.6 eV to ∼ 1.2 eV. More interestingly, in the kinetic process involving the moving of the bottom S layer as shown in Figs. 4(b) and 4(d), the energy barriers are further substantially reduced to ∼ 0.7 eV. For both cases, the optimized transition states correspond to the moving S atoms located nearly at the bridge sites of the central Mo/W layer. The energy barriers to move the bottom S layer are smaller than the barrier of a freestanding monolayer MoS_2 transforming from the 1T′ phase to the 1H phase (∼ 0.9 eV).[39]

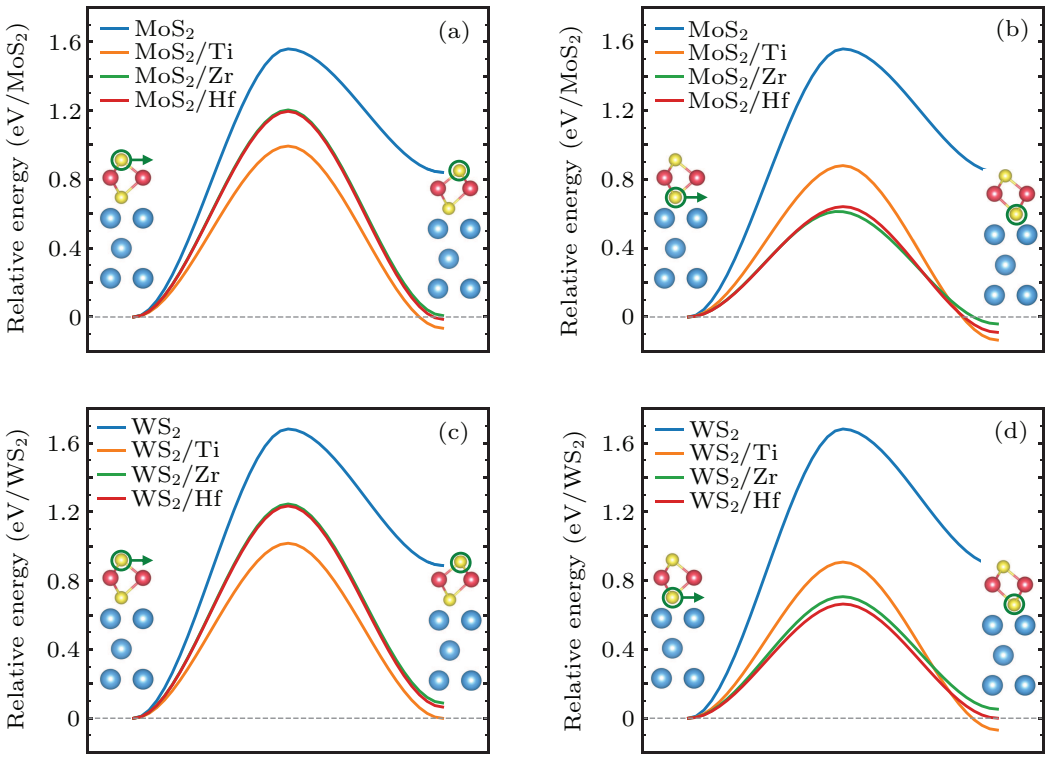


Fig. 4. Two possible phase transformation pathways from the 1H phase to the 1T phase. (a) MoS_2 with the moving of the top S layer, (b) MoS_2 with the moving of the bottom S layer, (c) WS_2 with the moving of the top S layer, (d) WS_2 with the moving of the bottom S layer. In all plots, the green circles and arrows attached to S atoms indicate the moving atom and the direction of atomic motion during the process of the phase transformation.

Such a 1T′ to 1H phase transformation has been demonstrated to be experimentally accessible for MoS_2.[28,29] All these results indicate that the proposed metal substrates can effectively facilitate the phase transformation of adsorbed MoS_2 and WS_2 monolayers from the 1H phase to the 1T′/1T phase.

3.3. Substrate effects on the hydrogen evolution reaction

We next investigate the catalytic activity of the 1T′-MoS_2 and 1T′-WS_2 monolayers with the support of the metal substrates. Different from the 1T′ phase achieved by ion intercalation, the top surface of the TMDs monolayers is still freely exposed for the chemical reaction. In addition, the metal substrates can be used directly as an electrode. Therefore, such a combined system is an ideal setup for the electrocatalytic HER.

It has been commonly recognized that the catalytic performance of an HER is essentially dictated by the Gibbs free energy (ΔG_H) of H adsorption on the catalysts with a value around zero being optimal.[40] For this reason and simplicity, we calculated the Gibbs free energies of atomic hydrogen adsorption on the metal substrate supported MoS_2 and WS_2 monolayers with 4×4 supercells as a measure. The calculation results are summarized in Table 3. For freestanding MoS_2, the basal plane of the 1H phase is catalytically inert, $\Delta G_H = 1.92$ eV, while the 1T′ phase is active, with a ΔG_H of 0.19 eV. In the presence of the metal substrates, the ΔG_H of 1H-MoS_2 is reduced to ~ 1.5 eV, but still too large for the HER. For 1T′-MoS_2, although their ΔG_H are generally increased by the metal substrates, the ΔG_H of 1T′-MoS_2 with Zr and Hf substrates are 0.48 eV and 0.56 eV, respectively, which are still comparable to the ΔG_H of Au (~ 0.5 eV).[41] For the case of 1T′-MoS_2/Ti, the ΔG_H increases to 1.30 eV, which may be related to the large lattice mismatch. For the cases of 1T′-WS_2, their ΔG_H are always larger than those of 1T′-MoS_2 on the same metal substrate, among which the 1T′-WS_2/Zr system has the lowest ΔG_H as large as 0.75 eV. To sum up, MoS_2 with Zr or Hf as the substrate may be considered as a promising HER catalyst.

Table 3. The Gibbs free energy (ΔG_H) of the hydrogen evolution reaction for 4×4 TMDs supercell with and without the metal substrates at 1/16 H coverage.

TMDs	Substrate	1H (eV)	1T′ (eV)
MoS_2	freestanding	1.92	0.19
	Ti (0001)	1.73	1.30
	Zr (0001)	1.36	0.48
	Hf (0001)	1.42	0.56
WS_2	freestanding	2.17	0.31
	Ti (0001)	1.99	1.51
	Zr (0001)	1.71	0.75
	Hf (0001)	1.79	0.82

Overall, the metal substrates reduced the ΔG_H of the 1H phase and increased the ΔG_H of the 1T′ phase. According to previous studies on freestanding TMDs,[42,43] the strength of H adsorption on the surface of TMDs is determined by the ability of the surface chalcogen atoms to attract electrons from H, and ΔG_H closely correlates to the position of the lowest unoccupied state of the catalyst (the conduction band minimum for semiconductors or the Fermi level for metals) with respect to the vacuum level. To examine its validity in our systems, we plot ΔG_H *versus* the lowest unoccupied state position ε_{LUS}, which is calculated as the energy difference of the vacuum level and the conduction band minimum for freestanding MoS_2 (WS_2) or the Fermi level for MoS_2 (WS_2) in the presence of the metal substrates. As shown in Fig. 5, an obvious linear correlation is revealed, which in consistent with the previous work,[42,43] and also indicates that ε_{LUS} is still a significant determinant for the HER of MoS_2 (WS_2) on the metal substrates. In addition, compared with the freestanding monolayer MoS_2 (WS_2), the values of ε_{LUS} increase for the 1T′ phase and decrease for the 1H phase in the presence of the metal substrates, which can be attributed to the interaction and charge transfer between the MoS_2 (WS_2) and the metal substrates.

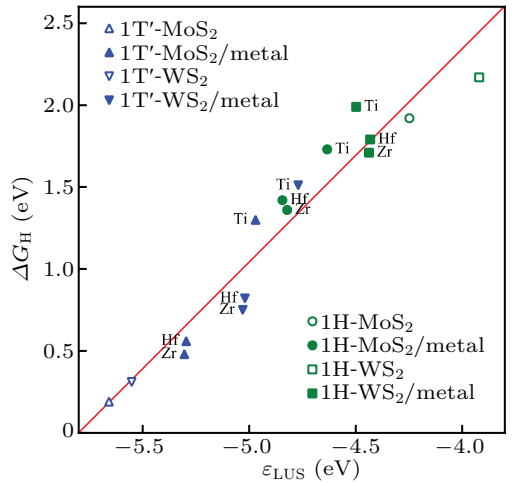


Fig. 5. Correlation between the Gibbs free energy ΔG_H and the lowest unoccupied state ε_{LUS}, which is calculated as the energy difference of the vacuum level and the conduction band minimum for freestanding MoS_2 (WS_2) or the Fermi level for MoS_2 (WS_2) in the presence of the metal substrates.

4. Conclusions

In summary, we have demonstrated from both energetics and kinetics aspects that low-work-function metals Ti, Zr, and Hf can be used as a functional substrate to effectively make monolayer MoS_2 and WS_2 undergo structural transformation from the 1H phase to the 1T′/1T phase, based on DFT calculations. In addition, 1T′-MoS_2 with Zr or Hf as a substrate may function as a potential catalyst for the HER.

Acknowledgment

Computational support was provided by National Supercomputing Center in Tianjin.

References

[1] Manzeli S, Ovchinnikov D, Pasquier D, Yazyev O V and Kis A 2017 *Nat. Rev. Mater.* **2** 17033
[2] Mak K F and Shan J 2016 *Nat. Photon.* **10** 216
[3] Xu X, Yao W, Xiao D and Heinz T F 2014 *Nat. Phys.* **10** 343
[4] Chhowalla M, Shin H S, Eda G, Li L-J, Loh K P and Zhang H 2013 *Nat. Chem.* **5** 263
[5] Wang Q H, Kalantar-Zadeh K, Kis A, Coleman J N and Strano M S 2012 *Nat. Nanotechnol.* **7** 699
[6] Enyashin A N, Yadgarov L, Houben L, Popov I, Weidenbach M, Tenne R, Bar-Sadan M and Seifert G 2011 *J. Phys. Chem. C* **115** 24586
[7] Jaramillo T F, Jørgensen K P, Bonde J, Nielsen J H, Horch S and Chorkendorff I 2007 *Science* **317** 100
[8] Hinnemann B, Moses P G, Bonde J, Jørgensen K P, Nielsen J H, Horch S, Chorkendorff I and Nørskov J K 2005 *J. Am. Chem. Soc.* **127** 5308
[9] Yu Y, Nam G H, He Q, *et al.* 2018 *Nat. Chem.* **10** 638
[10] Geng X, Sun W, Wu W, Chen B, Al-Hilo A, Benamara M, Zhu H, Watanabe F, Cui J and Chen T 2016 *Nat. Commun.* **7** 10672
[11] Chang K, Hai X, Pang H, Zhang H, Shi L, Liu G, Liu H, Zhao G, Li M and Ye J 2016 *Adv. Mater.* **28** 10033
[12] Chou S S, Sai N, Lu P, Coker E N, Liu S, Artyushkova K, Luk T S, Kaehr B and Brinker C J 2015 *Nat. Commun.* **6** 8311
[13] Fan X L, Yang Y, Xiao P and Lau W M 2014 *J. Mater. Chem. A* **2** 20545
[14] Voiry D, Salehi M, Silva R, Fujita T, Chen M, Asefa T, Shenoy V B, Eda G and Chhowalla M 2013 *Nano Lett.* **13** 6222
[15] Huang H H, Fan X, Singh D J and Zheng W T 2020 *Nanoscale* **12** 1247
[16] Xiao Y, Zhou M, Liu J, Xu J and Fu L 2019 *Sci. China Mater.* **62** 759
[17] Wang R, Yu Y, Zhou S, Li H, Wong H, Luo Z, Gan L and Zhai T 2018 *Adv. Funct. Mater.* **28** 1802473
[18] Voiry D, Mohite A and Chhowalla M 2015 *Chem. Soc. Rev.* **44** 2702
[19] Lin Y C, Dumcenco D O, Huang Y S and Suenaga K 2014 *Nat. Nanotechnol.* **9** 391
[20] Liu L, Wu J, Wu L, Ye M, Liu X, Wang Q, Hou S, Lu P, Sun L, Zheng J, Xing L, Gu L, Jiang X, Xie L and Jiao L 2018 *Nat. Mater.* **17** 1108
[21] Gao P, Wang L, Zhang Y, Huang Y and Liu K 2015 *ACS Nano* **9** 11296
[22] Wang L, Xu Z, Wang W and Bai X 2014 *J. Am. Chem. Soc.* **136** 6693
[23] Lukowski M A, Daniel A S, Meng F, Forticaux A, Li L and Jin S 2013 *J. Am. Chem. Soc.* **135** 10274
[24] Duerloo K A N, Li Y and Reed E J 2014 *Nat. Commun.* **5** 4214
[25] Yin X, Tang C S, Wu D, Kong W, Li C, Wang Q, Cao L, Yang M, Chang Y H, Qi D, Ouyang F, Pennycook S J, Feng Y P, Breese M B H, Wang S J, Zhang W, Rusydi A and Wee A T S 2019 *Adv. Sci.* **6** 1802093
[26] Ouyang B, Xiong S and Jing Y 2018 *npj 2D Mater. Appl.* **2** 13
[27] Ling F, Jing H, Chen Y, Kang W, Zeng W, Liu X, Zhang Y, Fang L and Zhou M 2018 *J. Mater. Chem. C* **6** 12245
[28] Ji X, Wu C, Deng J, Li J and Jin C 2020 *Appl. Phys. Lett.* **116** 033103
[29] Eda G, Yamaguchi H, Voiry D, Fujita T, Chen M and Chhowalla M 2011 *Nano Lett.* **11** 5111
[30] Kresse G and Furthmüller J 1996 *Phys. Rev. B* **54** 11169
[31] Blöchl P E 1994 *Phys. Rev. B* **50** 17953
[32] Kresse G and Joubert D 1999 *Phys. Rev. B* **59** 1758
[33] Perdew J P, Burke K and Ernzerhof M 1996 *Phys. Rev. Lett.* **77** 3865
[34] Methfessel M and Paxton A T 1989 *Phys. Rev. B* **40** 3616
[35] Henkelman G, Uberuaga B P and Jónsson H 2000 *J. Chem. Phys.* **113** 9901
[36] Grimme S, Antony J, Ehrlich S and Krieg H 2010 *J. Chem. Phys.* **132** 154104
[37] Grimme S, Ehrlich S and Goerigk L 2011 *J. Comput. Chem.* **32** 1456
[38] Nørskov J K, Bligaard T, Logadottir A, Kitchin J R, Chen J G, Pandelov S and Stimming U 2005 *J. Electrochem. Soc.* **152** J23
[39] Guo Y, Sun D, Ouyang B, Raja A, Song J, Heinz T F and Brus L E 2015 *Nano Lett.* **15** 5081
[40] Benck J D, Hellstern T R, Kibsgaard J, Chakthranont P and Jaramillo T F 2014 *ACS Catal.* **4** 3957
[41] Michalsky R, Zhang Y J and Peterson A A 2014 *ACS Catal.* **4** 1274
[42] Liu Y, Wu J, Hackenberg K P, Zhang J, Wang Y M, Yang Y, Keyshar K, Gu J, Ogitsu T, Vajtai R, Lou J, Ajayan P M, Wood B C and Yakobson B I 2017 *Nat. Energy* **2** 17127
[43] Wang J, Liu J, Zhang B, Ji X, Xu K, Chen C, Miao L and Jiang J 2017 *Phys. Chem. Chem. Phys.* **19** 10125